Nonstationary impact of ENSO on Euro-Atlantic winter climate

Richard J. Greatbatch, Jian Lu and K. Andrew Peterson

Department of Oceanography, Dalhousie University, Halifax, Nova Scotia, Canada B3H 4J1

Abstract.

Previous studies have suggested a lack of robustness over the Euro-Atlantic sector in the extratropical teleconnection response to ENSO. We use a simple AGCM to show that during the 20 years before and after the late 1970's, the ENSO signal leaving the tropics has the character of a wave train that is similar to the PNA, but is much stronger and penetrates further poleward in the post 1970's period. We also find that the synchronous extratropically-forced model response is almost the reverse in the post- compared to the pre-late 1970's period. We suggest that the nonstationarity in the ENSO teleconnection is due primarily to the sensitivity of the tropically-forced signal to subtle details of the tropical forcing. The extent to which the extratropically-forced response is itself dependent on the tropical forcing, or simply the result of chance, is not clear.

1. Introduction

The El Niño-Southern Oscillation (ENSO) phenomenon has been extensively studied. One reason is the teleconnection response of ENSO to midlatitudes and the potential this offers for seasonal prediction (e.g. *Stockdale* [2000]). While the association between ENSO and climate anomalies over the Pacific basin and North America is well known (e.g. *Trenberth et al.* [1998]), the ENSO impact on the Euro-Atlantic region is more uncertain, but also sometimes important (see *Dong et al.* [2000]). In what we call the "canonical" Euro-Atlantic impact of ENSO, composites of the difference in winter mean sea level pressure (SLP) over the Euro-Atlantic sector for warm minus cold events indicate a statistically significant signal with a positive anomaly over northeastern Europe and a negative anomaly in a zonal belt stretching from the east coast of the United States to the Black Sea, reminiscent of the negative NAO [*Fraedrich and Müller* [1992]; *Fraedrich* [1994]; *Merkel and Latif* [2002]]. Nevertheless, the impact of ENSO on the Euro-Atlantic sector is not robust on interdecadal time scales [*van Loon and Madden* [1981]]. For example, *Rogers* [1984] found the canonical response in SLP data from 1940-79, but found a somewhat different signal during the period 1900-39. Recently, *Rimbu et al.* [2003] detected a shift in the late 1970's in the relationship between ENSO and a Red Sea coral record and attributed the shift to non-stationarity in the ENSO teleconnection pattern. A related non-stationarity between ENSO and rainfall over Israel has been reported by *Price et al.* [1998], and *Mariotti et al.* [2002] and *Rodo et al.* [1997] report further evidence of non-stationarity between ENSO and rainfall over Europe. The non-stationarity can also be seen in the running cross-correlation between the winter mean Tahiti-Darwin SO index (*Trenberth and Caron* [2000], hereafter, SOI) and the index of winter mean Cold Ocean Warm Land pattern (COWL, as defined by *Wallace et al.* [1996]) shown in Figure 1 (solid line). An abrupt change in the cross-correlation occurred around the 1970's, after which the two indices became anti-correlated at the 5% significant level. A negative correlation between the SOI and COWL implies a tendency for the Icelandic low to be deeper during the warm phase of ENSO, similar to the positive phase of the NAO, and in contrast to the canonical ENSO response noted above. Here, we choose two adjacent 20-year time windows 1958-77 and 1978-97 to represent the de-correlated and correlated periods between ENSO and COWL. These are also the two time periods used by *Hilmer and Jung* [2000] to study the eastward shift in the NAO. Following the convention of Hilmer and Jung, we refer to the time periods 1958-77 (1978-97) as P1 (P2). The main objective of this study is to investigate the non-stationary influence of ENSO on the extratropical atmospheric circulation, especially over the Euro-Atlantic sector. Sets of model experiments have been conducted and provide insight into the possible mechanisms for the nonstationarity of ENSO impacts in terms of the relative roles played by tropical and extratropical model forcings.

2. Regression Analysis

We begin by applying a regression analysis to winter (DJF) mean SLP and 1000mb air temperature taken from the NCAR/NCEP reanalysis (*Kistler et al.* [2001]) for 1948/49 to 1998/99. The regression pattern of SLP against the SOI for all 51 winters 1949-99 is almost identical to that reported by *Trenberth and Caron* [2000] (their Fig.4d) and is not shown here. Applying the regression to the P1 and P2 time windows yields the patterns shown in Fig.2a and b, where the contour (color shading) indicates the regression coefficients of SLP (1000mb temperature). The features in common between the two periods are a high pressure anomaly over the northeastern Pacific and a low pressure anomaly to the southwest of it, and an associated tripolar temperature anomaly pattern that is accounted for by the advection of the climatological mean temperature gradient by the anomalous geostrophic wind. Nevertheless, the North Pacific SLP dipole differs substantially between the two regression periods. During period P2, the positive pole has been much expanded and strengthened while the negative pole weakened and displaced compared to P1. What is more striking is the difference over the North Atlantic and European sectors. During P1, the SLP regression pattern is

Paper number .
0094-8276/03/$5.00

characteristic of a meridional dipole with negative values to the north and positive values to the south, reminiscent of the positive phase of the NAO, and in keeping with the canonical response to ENSO (e.g. *Fraedrich and Müller* [1992]). After the 1970's, the SLP signal flips its sign, consistent with the emergent link between ENSO and COWL shown in Figure 1. A student-t test indicates that only in very limited areas is the reversal of the relationship to ENSO significant (not shown). For example, the 1000mb temperature to the southwest of the Red Sea is significantly anticorrelated(correlated) with SOI during P1(P2). This result is in keeping with the changing relationship between the Red Sea coral record and Niño3 SST index from the pre-1970's to the post-1970's described by *Rimbu et al.* [2003].

3. Model Experiments and Results

The model is the same as that used in *Peterson et al.* [2002]. It is a simplified primitive equation model [*Hall* [2000]] for a dry, dynamical atmosphere driven by a constant forcing diagnosed from NCAR/NCEP reanalysis data. The forcing is calculated separately for each winter by initializing the unforced model with the observed daily mean states and averaging the implied time tendencies. An ensemble of 30 model experiments is carried out for each winter separately, the ensemble members differing only in the choice of initial condition. Each ensemble member is integrated for 4 months and the analysis is carried out on the final 3 months. Sets of ensembles have been carried out with the forcing varying from winter to winter over the whole globe, only in the tropical band equatorward of 36°N/S, and only in the extratropics poleward of 36°N/S (in the latter two cases, the forcing is held at the average over all 51 winters in the remaining part of the domain). The reasons for choosing 36°N/S as the separation latitude between the tropics and the extratropics has been discussed by *Greatbatch et al.* [2003].

Figures 3a,b show the ENSO teleconnection patterns during P1 and P2 in the globally forced case. The patterns are derived by regressing the model ensemble mean SLP for each winter against the observed SOI during P1 (Fig.3a) and P2 (Fig.3b). Comparing with Figure 2, we see that the model realistically captures the observed ENSO teleconnection pattern in each time window. Figures 3c,d show the corresponding model results when the forcing varies from winter to winter only in the tropics. We see that the tropical signal is broadly similar in both P1 and P2, with a PNA-like wave train (negative phase) emanating from the subtropical western Pacific in both time periods. However, the amplitude of the signal is 2 or 3 times greater in P2 than in P1. Results from a companion model linearized about the climatological mean circulation for all 51 winters show that this difference in amplitude is a feature of linear dynamics. Close inspection of the model forcing in the tropics does not reveal any similar increase in the amplitude of the model forcing between P1 and P2 (see Figure 4). On the other hand, *Branstator* [1985] has reported a strong sensitivity in the extratropical response to the spatial pattern of the tropical forcing, and it seems likely that the dramatically different amplitude in the model response between P1 and P2 is due to subtle differences in the spatial pattern of the tropical forcing. Given that the trend between P1 and P2 was towards a warmer tropical Pacific [*Trenberth et al.* [2002]], the increase in amplitude is also consistent with *Hoerling et al.* [2001] who find a stronger response for warm versus cold events. Also evident is the greater poleward penetration of the signal in P2. Consequently, the signal emerging from the tropics bears a strong resemblance to the COWL pattern (*Wallace et al.* [1996]) during P2. In fact, Figure 1 shows that the cross-relation between the SOI and the COWL index for the tropically-forced ensemble mean model response increases dramatically between P1 and P2, with up to 60 % of the variance in the tropically-emergent SOI signal being accounted for by COWL during P2. Furthermore, there is no significant correlation in either P1 or P2 between the SOI and the COWL index for the extratropically forced model runs. It follows that the significant correlation between the SOI and COWL during P2 noted in the NCAR/NCEP data can attributed to the change in the signal emerging from the tropics between P1 and P2.

The teleconnection patterns of ENSO driven by the extratropical model forcing are shown in Figures 3e,f. These plots are derived by regression of ensemble mean SLP against the observed SOI when the model forcing varies from winter to winter only in the extratropics. Again we see a dramatic difference between P1 and P2. Interestingly, the extratropically-driven SLP pattern congruent with ENSO during both periods resembles the Arctic Oscillation (AO: *Thompson et al.* [1998]), but with the sign reversed in P2 compared to P1. In P1, the ENSO-AO relationship suggested by Figure 3e is consistent with the canonical ENSO-Europe relationship (as can be seen when the pattern in Figure 3e is added to that in Figure 3c), whereas during P2 the extratropically-forced signal acts oppositely. (Note that the teleconnection patterns shown in Figure 3a,b are given, to a very good approximation, by simply adding the regression patterns shown in Figures 3c,d to those in Figures 3e,f, indicating the importance of linear dynamics.) An important issue is whether the extratropical model forcing that is responsible for the patterns shown in Figures 3e,f is itself a mid-latitude response to the tropically-driven signal shown in Figure 3c,d, (e.g. due to latent heat release in the mid-latitude storm tracks), or is the difference between Figures 3e,f simply the result of chance? While this question cannot be answered definitively, we note that there are regions where the patterns shown in Figures 3e,f are statistically significant, suggestive of a genuine link with ENSO, but one that is difficult to extract because of the dominance of other modes of variability at mid-latitudes.

4. Summary and Discussion

The link between ENSO and the Euro-Atlantic sector is not robust on interdecadal time scales (*van Loon and Madden* [1981]). An example is given in Figure 1 where we show the running cross-correlation between the SO and COWL indices. The emergence of a significant anticorrelation between the SOI and COWL after the 1970's is not consistent with the canonical response to ENSO over the Euro-Atlantic sector documented by *Fraedrich and Müller* [1992]. By using a simple dynamical model, we have shown that the ENSO-related signal emerging from the tropics was between 2 and 3 times stronger in amplitude during P2 (1978-97) than during P1 (1958-77), as well as showing a greater poleward penetration during the later period that explains the emergent link with COWL. Model experiments also show that the extratropically forced model response congruent with ENSO

resembles the AO pattern in both periods, but with the sign reversed, reinforcing the canonical ENSO response during P1 but countering it during P2. We suggest that the change in the extratropically-forced model response may partly be a consequence of the change in the ENSO signal emergent from the tropics, while recognising that it may also have arisen by chance alone.

Acknowledgments. We are grateful for funding from NSERC, CFCAS and CICS in support of the Canadian CLIVAR Research Network. We would also like to acknowledge H. Lin, J. Derome, and N.M.J. Hall for providing the model and the 51 years of model forcing computed from the NCAR/NCEP data.

References

Branstator, G., Analysis of general circulation model sea-surface temperature anomaly simulations using a linear model. Part I: Forced solutions, *J. Atmos. Sci.*, 42, 2225-2241, 1985.

Dong, B.W., R.T. Sutton, S.P. Jewson, A. O'Neill and J.M. Slingo, Predictable winter climate in the North Atlantic sector during the 1997-1999 ENSO cycle, *Geophys. Res. Lett.,* , 27, 985-988, 2000.

Fraedrich, K., An ENSO impact on Europe? *Tellus*, 46A, 541-552, 1994.

Fraedrich, K., and K. Müller, Climate anomalies in Europe associated with ENSO extremes, *Int. J. Climatol.*, 12, 25-31, 1992.

Greatbatch, R.J., H. Lin, J. Lu, K.A. Peterson and J. Derome, Tropical/Extratropical forcing of the AO/NAO: A corrigendum, *Geophys. Res. Lett.,* , 30(14) 1738, doi:10.1029/2003GL017406.

Hall, N. M. J., A simple GCM based on dry dynamics and constant forcing, *J. Atmos. Sci.,* 57, 1557-1572, 2000.

Hilmer M. and T. Jung, Evidence for a recent change in the link between the North Atlantic Oscillation and Arctic sea ice export, *Geophys. Res. Lett.,* 27, 989-992, 2000.

Hoerling, M.P., A. Kumar and T. Xu, Robustness of the nonlinear climate response to ENSO's extreme phases, *J. Climate*, 14, 1277-1293, 2001.

Kistler, R., W. Collins, S. Saha, G. White, J. Woollen, E. Kalnay, M. Chelliah, W. Ebisuzaki, M. Kanamitsu, V. Kousky, H. van den Dool, R. Jenne, M. Fiorino, The NCEP-NCAR 50-Year Reanalysis: Monthly Means CD-ROM and Documentation, *Bull. Am. Meteorol. Soc.,* 82, 247-268, 2001.

Mariotti, A., N. Zeng and K.-M. Lau, Euro-Mediterranean rainfall and ENSO - a seasonally varying relationship, *Geophys. Res. Lett.,* , 29, 10.1029/2001GL014248, 2002.

Merkel, U., and M. Latif, A high resolution AGCM study of the El Nino impact on the North Atlantic/European sector, *Geophys. Res. Lett.,* , 29, 1291, doi:10.1020/2001GL013726, 2002.

Peterson, K.A., R.J. Greatbatch, J. Lu, H. Lin and J. Derome, Hindcasting the NAO using diabatic forcing of a simple AGCM, *Geophys. Res. Lett.,* 29 (9), doi:10.1029/2001GL014502, 2002.

Price, C., L. Stone, A. Huppert, B. Rajagopalan and P. Alpert, A possible link between El Nino and precipitation in Israel, *Geophys. Res. Lett.,* , 25, 3963-3966, 1998.

Rimbu, N., G. Lohmann, T. Felis and J. Pätzold, Shift in ENSO teleconnections recorded by a northern Red Sea coral, *J. Climate*, 16, 1414-1422, 2003.

Rodo, X., E. Baert and F.A. Comin, Variations in seasonal rainfall in Southern Europe during the present century: relationships with the North Atlantic Oscillation and the El Nino-Southern Oscillation, *Climate Dynamics*, 13, 275-284.

Rogers, J.C., The Association between the North Atlantic Oscillation and the Southern Oscillation in the Northern Hemisphere, *Mon. Wea. Rev.*, 112, 1999-2015, 1984.

Stockdale, T.N., An overview of techniques for seasonal forecasting, *Stochastic Environmental Research and Risk Assessment*, 14, 305-318, 2000.

Thompson, D.W.J, and J.M. Wallace, The Arctic Oscillation signature in wintertime geopotential height and temperature fields, *Geophys. Res. Lett.,* 25, 1297-1300, 1998.

Trenberth, K.E., G.W. Branstator, D. Karoly, A. Kumar, N.-C. Lau and C. Ropelewski, Progress during TOGA in understanding and modeling global teleconnections associated with tropical sea surface temperatures, *J. Geophys. Res.*, 103 (C7), 14,291-14,324, 1998.

Trenberth, K.E., and J.M. Caron, The Southern Oscillation revisited: sea level pressures, surface temperatures, and precipitation, *J. Climate*, 13, 4358-4365, 2000.

Trenberth, K.E., J.M. Caron, D.P Stephaniak and S. Worley, Evolution of El Nino-Southern Oscillation and global atmospheric surface temperatures, *J. Geophys. Res.*, 107, doi:10.1029/2000/D000298, 2002.

van Loon, H., and R.A. Madden, The Southern Oscillation. Part I: Global associations with pressure and temperature in northern hemisphere winter, *Mon. Wea. Rev.*, 109, 1150-1162, 1981.

Wallace, J. M., Y. Zhang and L. Bajuk, Interpretation of interdecadal trends in Northern Hemisphere surface air temperature. *J. Clim.,* 9, 249-259, 1996.

R.J. Greatbatch, J. Lu and K. A. Peterson, Department of Oceanography, Dalhousie University, Halifax, NS, Canada, B3H 4J1. (richard.greatbatch@dal.ca)

(Received _____.)

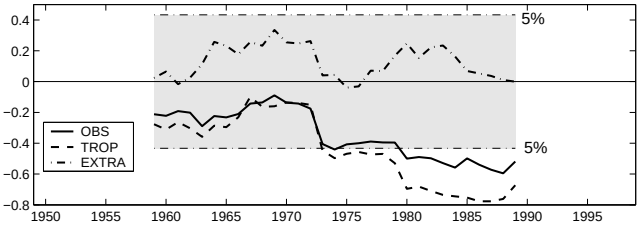

Figure 1. Running cross-correlation using a 21 year window between the observed SOI and the COWL index computed from the NCAR/NCEP data (solid line), and the ensemble mean tropical (dashed) and extratropical (dot-dash) forced model runs. The unshaded region marks the 5% significance level.

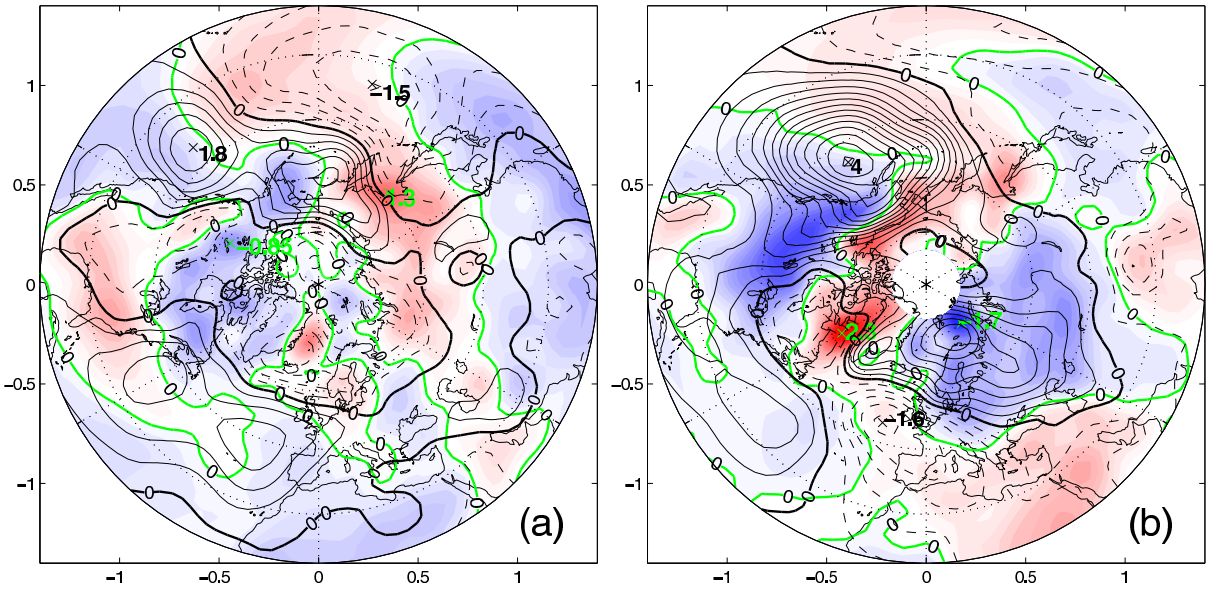

Figure 2. (a) and (b) are linear regression of NCAR/NCEP SLP (contours) and 1000mb temperature (color shading) against the SOI during P1 and P2 respectively. The zero isolines of the SLP (1000mb temperature) pattern are highlighted by thick black (green) lines. The contour interval is 0.3hPa/0.3°C.

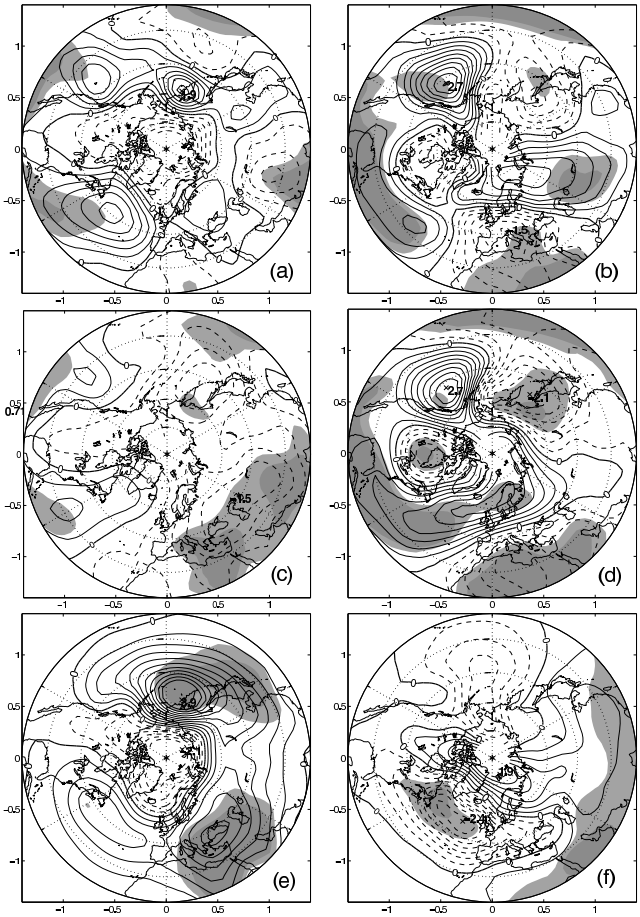

Figure 3. Linear regression against the observed SOI of the ensemble mean SLP from the model for global (a,b), tropical (c,d) and extratropical forcing (e,f) in P1 (a,c,e) and P2 (b,d,f). The grey shading indicate the 5% significance level. The contour interval is 0.3 hPa.

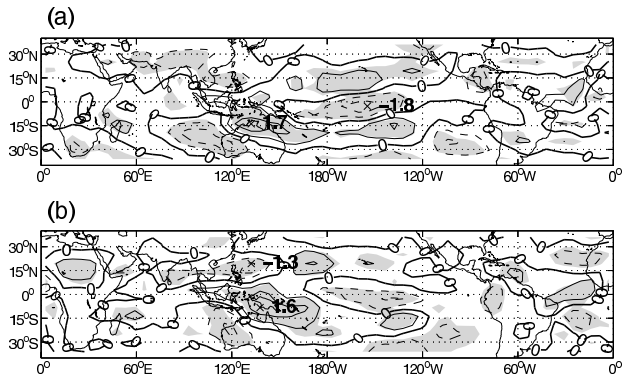

Figure 4. Regression of the vertically averaged forcing for the temperature equation against the observed SOI during P1 (panel a) and P2 (panel b). The 5% significant level is denoted by grey shading. The contour interval is 0.6°C per day.